Highlights

Spatial and Temporal Variability of Surface Deformation in a Paraglacial Alpine Environment Measured from Satellite Radars

Nicolas Oestreicher, Andrea Manconi, Clément Roques, Adriano Gualandi, Simon Loew

- Statistical signal decomposition for displacement timeseries in complex environment
- Satellites map irreversible long-term damage of stable and unstable slopes
- Spatial variations of reversible deformation linked to pore pressure change
- Local groundwater recharge deformation patterns are discernible from satellites

Spatial and Temporal Variability of Surface Deformation in a Paraglacial Alpine Environment Measured from Satellite Radars

Nicolas Oestreicher[a,b], Andrea Manconi[a,c], Clément Roques[d], Adriano Gualandi[e,f], Simon Loew[a]

[a] *Department of Earth Sciences, ETH Zürich, Sonneggstrasse 5, Zürich, 8092, Switzerland*
[b] *now at University of Geneva, Department of Earth Sciences, Geneva, Switzerland*
[c] *now at WSL Institute for Snow and Avalanche Research SLF, Climate Change, Extremes and Natural Hazards in Alpine Regions Centre CERC, Davos Dorf, Switzerland, Davos, Switzerland*
[d] *Centre for Hydrogeology and Geothermics (CHYN), University of Neuchâtel, Neuchâtel, Switzerland*
[e] *University of Cambridge, Department of Earth Sciences, Bullard Laboratories, Cambridge, United Kingdom*
[f] *Istituto Nazionale di Geofisica e Vulcanologia (INGV), Osservatorio Nazionale Terremoti (ONT), Roma, Italy*

Abstract

We study the deformation in the region of the Great Aletsch Glacier in the period 2015-2021. With the help of a statistical blind source separation method, we differentiate sub-centimetric displacements caused by environmental factors in the satellite radar interferometry time series. Long-term displacement trends in the vicinity of large slope instabilities potentially indicate slope reaction to the glacier's retreat and cyclic loadings. Annual cyclic deformation designates where considerable pore pressure variations occur in the fractured bedrock slopes related to groundwater storage-discharge processes. Spatial variations in the cyclic deformation exhibit variability in pore-pressure change and rock mass hydromechanical properties. We validate our observations drawn from satellites with a continuous ground monitoring network. The outcomes of this study show the potential of using satellite radar interferometry to investigate slope-scale mechanical processes driven by seasonal to multiannual environmental factors in an alpine context.

Keywords: deformation, groundwater, glacier retreat, paraglacial, Alps

Preprint submitted to Remote Sensing of Environment *January 22, 2024*

1. Introduction

Ground surface deformation in alpine environments results from multiple tectonic and environmental factors (Sternai et al., 2019). The deformation of the surface can inform us about processes happening at and below the surface, such as tectonic activity (Bock et al., 1993), gravitational instabilities (Agliardi et al., 2020), changes in surface loads (Mey et al., 2016), thermoelasticity of the subsurface (Collins et al., 2018), as well as poroelastic changes in aquifers (Loew et al., 2007; Vasco et al., 2019). Due to the amplified effects of climate change at high elevations, most glaciers are rapidly melting (Huss and Hock, 2018), exposing large areas to paraglacial conditions (Oliva et al., 2020). The deglaciated slopes are prone to develop instabilities, sometimes delayed after the glacier retreat due to the accumulation of progressive damage (Ballantyne et al., 2014; Grämiger et al., 2020). In this context, monitoring the surface deformation of such areas is critical to better understand where new slope instabilities could develop and how environmental factors could participate in their formation.

Measuring ground displacements at relevant spatial and temporal resolutions is challenging in alpine environments, mainly because of costs associated with the deployment of monitoring systems and the difficulties of accessing remote and hazardous places. Remote sensing has increased our capability to gain quantitative insights into the properties and dynamics of land surfaces globally. Among other methods, the continuous development of the Differential Interferometric Synthetic Aperture Radar (DInSAR) in the past decades allowed quantification of the ground motion (Rosen et al., 2000; Crosetto et al., 2016). Noteworthy, several recent examples have shown the capability of DInSAR to monitor movement related to changes in groundwater storage in different geographic settings (Béjar-Pizarro et al., 2017; Neely et al., 2021; Ali et al., 2022; Song et al., 2022). Applying DInSAR might be challenging in mountain environments because of the intrinsic limitations associated with snow cover, geometric distortions (layover and shadowing), and atmospheric phase screen (Wasowski and Bovenga, 2014; Manconi, 2021). The relatively low amplitude of expected seasonal deformation (centimetric) also challenges the use of DInSAR. However, with modern processing approaches and signal deconvolution techniques, we hypothesize that DInSAR can reveal key quantitative insights about surface displacement dynamics associated with mountain slope instabilities.

This work shows the result of surface displacement measured with DInSAR in the Aletsch valley, Switzerland (see Figure 1). This region is intensively studied as it hosts the current longest European Alps glacier that retreated over 1 km in length between 2′000 and 2′020 (GLAMOS - Glacier Monitoring Switzerland, 2021). The bedrock in the area is composed of strongly foliated gneisses and granite from the Aar massif (Berger et al., 2016). Several instabilities are identified around the glacier tongue (Kos et al., 2016; Glueer et al., 2019; Hugentobler et al., 2020), some being inactive, while others are moving at rates high enough to influence and interact with the glacier flow (Storni et al., 2020).

A large monitoring setup (see Figure 1) was installed in the Aletsch valley in 2013 and improved since, with Robotic Total Stations (RTS) and continuous Global Navigation Satellite Systems stations (cGNSS) (Frukacz et al., 2017; Glueer et al., 2021). Together with extensive fieldwork, the system helped to characterize the structures and kinematic model of the Moosfluh landslide (Glueer et al., 2020). The objectives of the monitoring network extend beyond the surveillance of the major instabilities and include the study of long-term progressive slope damage, landslide formation in glacial and para-glacial environments, hydro-mechanical landslide-glacier interactions and monitoring system development (Frukacz et al., 2017; Grämiger et al., 2017, 2018; Manconi et al., 2018; Glueer et al., 2019, 2020; Hugentobler et al., 2020; Storni et al., 2020; Grämiger et al., 2020; Hugentobler et al., 2021; Oestreicher et al., 2021; Glueer et al., 2021; Oestreicher et al., 2023). To increase the spatial and temporal coverage of the ground observation network, we have processed the available data acquired from the ESA Sentinel-1 constellation (Torres et al., 2012) in the period 2015-2021. We generated surface velocity maps and displacement time series with the interferometric point target analysis (IPTA) (Werner et al., 2003). The IPTA results have been further processed using an advanced signal decomposition method to link the main signal components with environmental controlling factors (Gualandi and Liu, 2021). We finally validated the DInSAR data analysis outcomes with ground-trusted data and previous site knowledge (Hugentobler et al., 2020; Grämiger et al., 2020; Oestreicher et al., 2021, 2023) and extended the spatio-temporal analysis of ongoing slope displacement processes into formerly unexplored regions in the lower Aletsch valley study area.

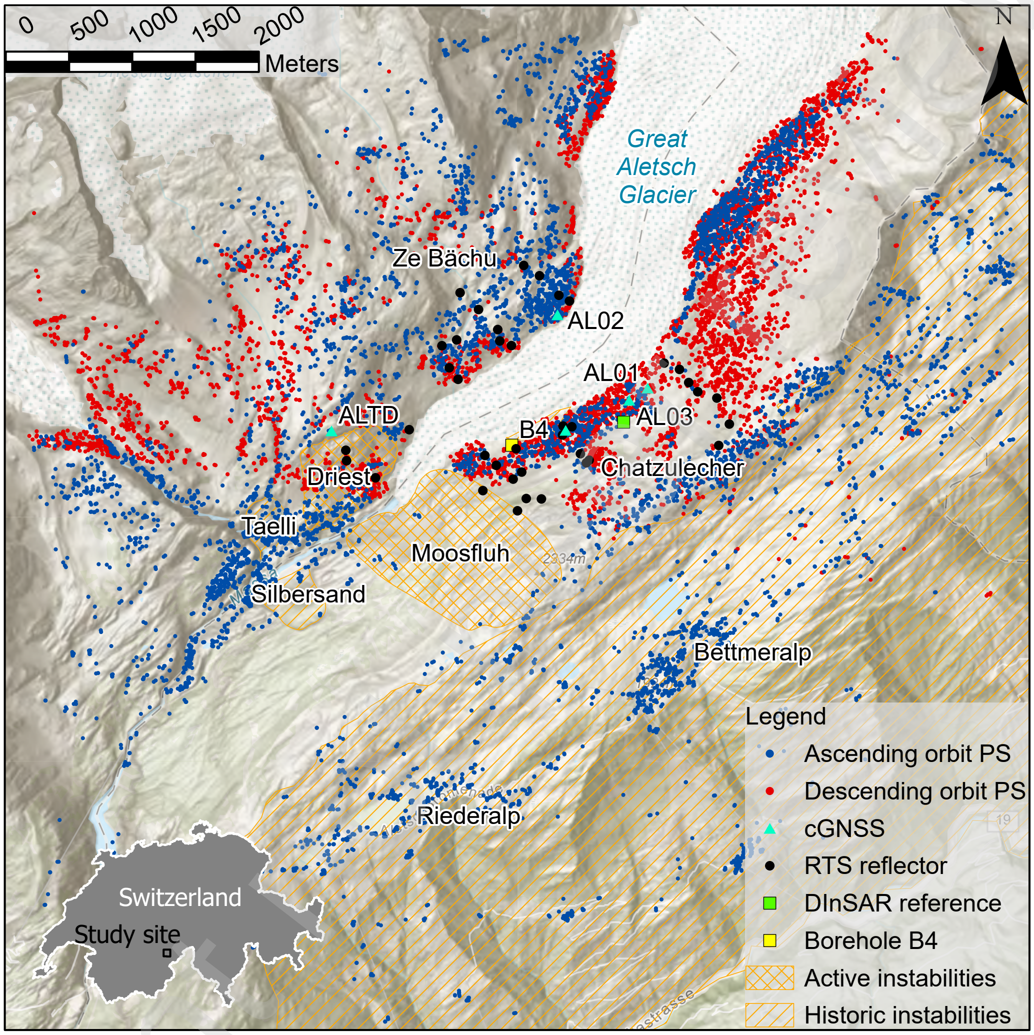

Figure 1: Study area with selected Persistent Scatterers (PS) for the analysis of the ascending (blue) and descending (red) orbits and the DInSAR reference point (green rectangle). cGNSS stations (cyan triangles), RTS reflectors (black points), and the borehole (yellow square) used in this study are drawn around the tongue of the Great Aletsch glacier, close to a range of large instabilities (orange patches). The location of the study area in Switzerland is shown in the bottom left corner.

2. Methods

2.1. Differential Interferometry of Synthetic Aperture Radar Data (DInSAR)

We considered the ESA Sentinel-1 imagery acquired during the period 2015-2021. A total of 329 images from the Track 15, Ascending orbit (hereafter T015A) and 346 from the Track 66, Descending orbit (hereafter T066D), were selected, and processed with the GAMMA software (Wegmüller et al., 2016). The images have been initially co-registered (aligned) to the dates Aug 08, 2018 (T015A) and Aug 26, 2018 (T066D), respectively. These images were also used to generate the interferometric pairs following the single reference approach, which has been demonstrated to be an effective method in alpine environments (Strozzi et al., 2017). Perpendicular baselines for all pairs are generally below 150 m, as expected for Sentinel-1 (See Table 1 and Table 2 in the supporting information). Topographic phase component was removed by considering the high-resolution digital elevation model provided by Swisstopo (SwissAlti3D), with a ground sampling distance of 5 m. The IPTA (Werner et al., 2003) strategy was applied to retrieve average surface velocities and displacement time series for point targets with high temporal correlation (coherence). Spatial and temporal filtering was applied to mitigate atmospheric artifacts and other system noise sources (Wegmüller et al., 2021). The final results include a total of 7′148 and 7′299 coherent point targets for the T015A and T066D orbits and a total of 329 and 346 scenes, respectively.

The IPTA dataset is then corrected for the motion of the reference point. We use the cGNSS data from the Chatzulecher station. We add the displacement of the cGNSS to the one measured from the satellite. Because the sampling from the satellite occurs every 6 d to 12 d depending on the number of available satellites, we first need to downsample the cGNSS data (the cGNSS station measures its position every 30 s). A daily solution is calculated with respect to another cGNSS station (HOHT) situated in Rhone Valley. An intermediate reference station (FIES), closer to Chatzulecher, is also involved in this process to reduce the atmospheric noise on the GNSS positioning. More details on this procedure are available in Limpach et al. (2016). However, the daily signal from the cGNSS still includes noise (both instrumental and atmospheric), particularly in the vertical direction. The latter is critical, as the incidence angle from the satellite is around 35° from the vertical for the study area. To increase the signal-to-noise ratio further, we average the cGNSS position in the 6 d preceding a satellite observation.

Then, we calculate the position of the cGNSS station in the line of sight (LOS) of the satellite d:

$$d = cos(\theta)l_U - sin(\theta)cos(\alpha)l_N - sin(\theta)sin(\alpha)l_E \quad (1)$$

where θ is the incidence angle (from vertical), α is the satellite flying direction (clockwise from North), and l_U, l_N, l_E are respectively, the Up, North, and East components of the GNSS position. Finally, the displacement of the reference point in the line of sight of the satellite is added to the displacement observed from the satellite in order to correct the satellite displacement data in the absence of any stable point in the area.

2.2. Validation with Ground-Truthing of Satellite Deformation

The slopes of the Aletsch Valley in our study area experience significant annual cyclic and reversible displacement of the slopes, as observed at many observation points (Oestreicher et al., 2021). Three monitoring boreholes were drilled near the ice margins (at the time of the installation) (Hugentobler et al., 2020). One of them provides information on the pore pressure fluctuations in the slope. All three are equipped to track sub-millimetric deformation along the depth ($\sim$50 m) of the boreholes (Hugentobler et al., 2020). Hugentobler et al. (2021) show that the shallower part of the slope reacts to temperature variations, while the deeper part reacts more to the variations of the slope groundwater table and englacial pore pressure fluctuations, resulting in reversible displacements. Irreversible displacements were also recorded and attributed mainly to the current unloading of the melting glacier and damage from cyclic loading (Hugentobler et al., 2022). To further test the validity of the results from the DInSAR processing, we make use of the extensive ground monitoring system in place in the Aletsch valley (Oestreicher et al., 2021), and we compare cGNSS and RTS displacement timeseries converted in the LOS with nearby satellite points in a circle around the stations. If the circle's radius is too small, only a few permanent scatterers (PSs) are retained, while if the radius is too large, the PSs have higher chances to experience different displacements than the displacement of the ground station. As a trade-off, we select a circle with a radius of 50 m (see Figure 2 and Figures S2, S3, S4, S5, S6 and S7 in the Supporting Information). We find a good correlation between the three methods. In particular, the long-term trends are well respected, and an extensive range of points exhibit seasonal patterns independently of the observation method.

The comparison between DInSAR and cGNSS stations' displacement shows that the two methods give similar results regarding long-term trends and seasonal displacements. Some cGNSS stations have data interruptions: the station AL01 was taken down by a snow avalanche in 2018 and replaced by the station AL03 at a safer location (Oestreicher et al., 2021). The number of PSs in 50 m circles around the cGNSS stations fluctuates from 0 to 20. In some cases (e.g., ALTS and ALTD in the ascending orbit), the displacement of the PSs deviates slightly from the one recorded by the cGNSS. Some of the deviations are due to the PS's location at a distance to the station, and local changes of the surface displacement between the location of the station and the PSs, as sometimes local displacement variations are significant (Oestreicher et al., 2021). Figure 2 shows that in some cases (e.g., AL01 and AL03 in the descending orbit), the IPTA method can fill up a gap in the cGNSS timeseries. The point-by-point comparison for the total station's data is available in the supporting information.

One of the differences between the IPTA and ground-based displacement observations is the presence of larger noise in the satellite data in winter. The snow covering the ground in winter introduces high variabilities in the phase values measured from the satellites. Instead of cutting out winter times from the analysis and/or from the final displacement timeseries, we keep elevated noise in the data. The reason is that some points might stay uncovered for longer periods in winter, for example, on steep cliffs or close to springs where the flowing groundwater melts the snow earlier than at other places. South-oriented slopes and low-elevation areas also see a shorter snow-covered period during winter time. Those points stay coherent longer during the year and are important to retrieve information about annual cyclic displacement.

2.3. Statistical Decomposition of Satellite Data

The displacement timeseries of a single PS have likely been generated by multiple sources of deformation. For example, a point on a mountain slope might be subject to gravitational slope deformation, as well as thermoelastic and poroelastic effects on the slope. Moreover, system noise and atmospheric artifacts can also be present. All these signals are mixed in the satellite displacement data, therefore requiring disentanglement. Statistical signal decomposition techniques are commonly used to isolate parts of the signal originating from different sources (Gaddes et al., 2018). Among the available methods, the Principal Component Analysis (PCA) is standard but often cannot properly separate physical sources into different components.

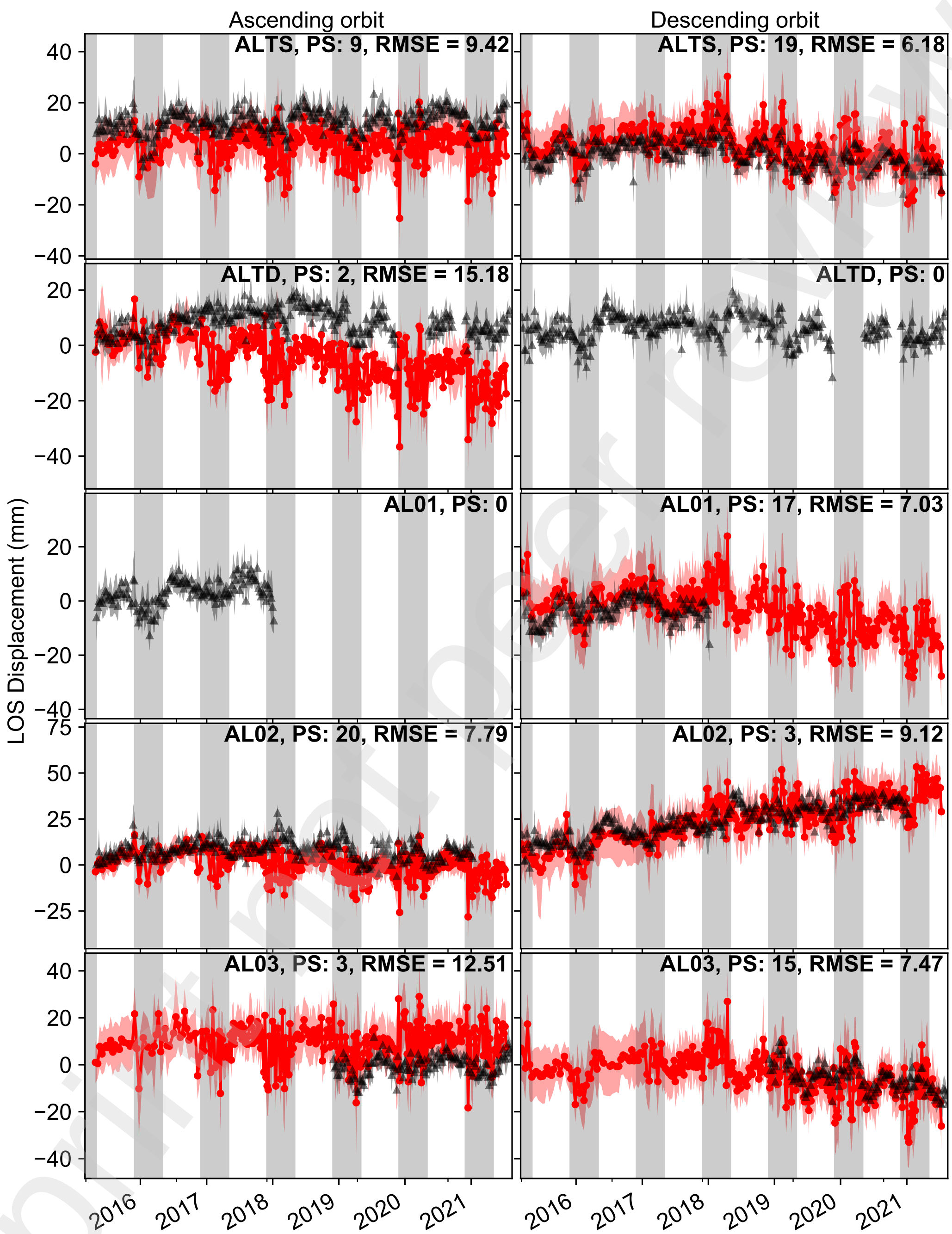

Figure 2: Comparison between cGNSS stations displacement (black) and nearby permanent scatterers (red) for the ascending (left) and descending (right) orbits in a circle of 50 m radius around each station. See Figure 1 for the location of the five cGNSS stations. PS is the number of permanent scatterers in the 50 m circle around cGNSS stations, RMSE is in mm. Grey zones mark times when the stations are susceptible to being snow-covered, inducing a larger scattering of the satellite recordings.

More advanced methods for blind source separation of DInSAR data include the Independent Component Analysis (ICA) (Ebmeier, 2016; Gaddes et al., 2018), and the variational Bayesian ICA (vbICA) (Gualandi and Liu, 2021), as well as deep learning autoencoders (Rouet-Leduc et al., 2021). The signal of interest (in the LOS of the satellite) extracted from the decomposition process consists of timeseries for each component at all permanent scatterers in the study area.

We use the vbICA, which statistically extracts Independent Components (ICs) from timeseries without a priori definition of the physical sources of the signal (Gualandi and Liu, 2021). Hereafter, we present the results of the vbICA in spatial mode (S-mode) with three ICs and whitening, meaning that the algorithm looks for independent components in the spatial domain and the data has been sphered to allow for an easier separation of almost parallel components. The variational Bayesian approach allows us to select the number of ICs following the Automatic Relevance Determination (ARD) method, as described by Choudrey and Roberts (2003); Gualandi and Liu (2021). We use the ratio between the maximum and minimum variance of the mixing matrix columns and retain the smallest number of components with a ratio lower than an arbitrary small threshold of this ratio fixed at 0.01 (see Figure S8 in the Supporting Information). Additional components do not significantly add information and can be neglected (Gualandi and Liu, 2021).

3. Surface Deformation of Valley Flanks from DInSAR

3.1. Location of Persistent Scatterers (PS) in the Study Area

Figure 1 shows measurement points for ascending and descending orbits. Both datasets are referenced to a point where the relative displacement is known, located close to the center of the $\sim 25\,\mathrm{km}^2$ study area (Figure 1). The reference point is relative to the reference cGNSS station HOHT, situated outside the study area in the Rhone valley. HOHT records an additional uplift of 2.1 mm/yr relative to the Swiss coordinate reference system CHTRF2016 (Oestreicher et al., 2021). 7′148 measurement points for the ascending orbit and 7′299 for the descending one were analyzed. The points of the ascending orbit spread further away from the reference point, particularly on the North flank of the Rhone valley, around the villages of Riederalp and Bettmeralp (Figure 1). For both datasets, no points are found on the glacier nor on the main part of the fast-moving Moosfluh landslide and small rock glacier East of AL03. This is because surface deformations in these regions are too rapid to ensure efficient tracking with the Sentinel 1 satellites, inducing decorrelation (Manconi et al., 2018; Manconi, 2021). The areas covered by forests (i.e., to the South-West of the Moosfluh instability) also lack points due to vegetation-induced decorrelation.

3.2. Irreversible Displacements

The displacement time series over the 2015-2021 time period are available for each measurement point in Figure 1. We first extract the long-term trend in the displacement time series that reveals the irreversible deformation affecting the valley flanks (Figure 3). The magnitude of the observed signal in the 6 yr dataset is up to 17 mm/yr in the descending orbit and around 8 mm/yr in the ascending orbit. The most significant surface velocities observed from the ascending and descending orbit take place at the main slope instabilities (Moosfluh, Driest, Riederalp-Bettmeralp) and on the South-East facing slopes at Ze Bächu (see Figure 3).

The ascending and descending orbits show large velocities North-East of the Moosfluh instability. The descending orbit is particularly well suited to detect the landslide's motion, going to the North-West and down, hence away from the satellite line of sight (Glueer et al., 2020). While there are almost no PS in the central, faster part of the Moosfluh instability, PS on some parts of the landslide moving slower are preserved. The significant displacement away from the satellite in the descending orbit, in the slopes on the right flank of the Moosfluh landslide, induces a cluster of negative values in the histogram of LOS displacement (Figure S10). The detection of motion on the right flank of the Moosfluh instability is confirmed by the reflectors situated in this part of the slope (see Figure S3), which show a progressive attenuation of the deformation with the distance to the lateral scarps which formed in 2016 (Glueer et al., 2020). This could be explained by the field observation of decreasing openings of tension cracks with distance from the lateral scarp to the North-East (Truttmann et al., 2021; Hugentobler et al., 2021).

The Driest instability exhibits points moving away from and towards the satellite, respectively, for the top and bottom parts of the instability. This is consistent with RTS data and the rotational nature of this suspended rockslide (Vogler, 2015). The Riederalp-Bettmeralp DSGSD shows an average displacement rate of 1.1 mm/yr away from the satellite in the ascending orbit (1446 PS) and 0.7 mm/yr towards the satellite in the descending orbit (149 PS) (Figure 3).

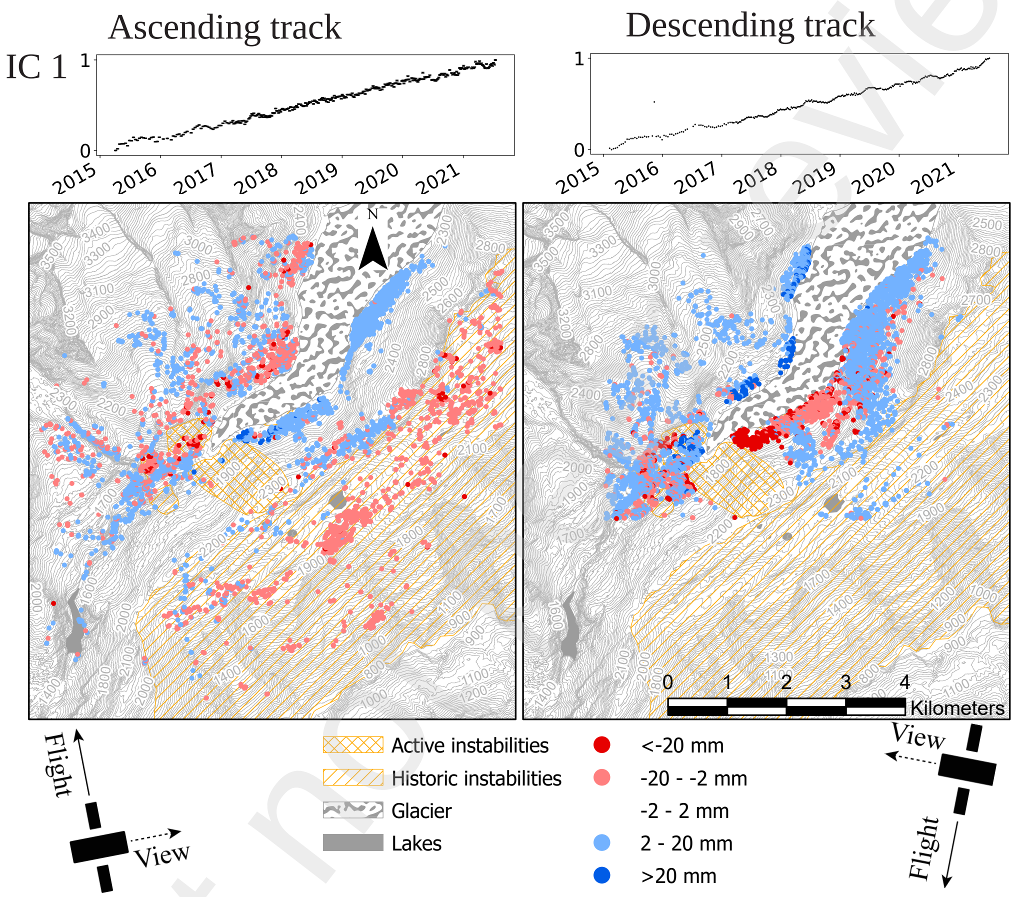

Figure 3: First independent component of vbICA for the ascending and descending tracks of the satellite. The upper panels show the time series of the IC. Positive values (blue colored dots) on the map signify displacement towards the satellite for a positive change in the time series. To reconstruct the displacement associated with the IC at a PS between two dates, multiply the value shown on the map by the difference in the time series of IC1 (upper panels) at the two given dates.

At other locations, for example, on the right flank of the valley along the glacier, significant long-term trends are detected and confirmed by cGNSS and RTS methods (see Figure S6 and S5). We observe displacement towards the valley center up to $\sim$7 mm/yr on both valley flanks in the recently deglaciated bedrock slopes. No slope instabilities are mapped at this location, and no signs of instabilities are visible in the field.

3.3. Reversible Deformation

The satellites detect seasonal cycles in deformation at a magnitude below the centimeter in the LOS direction (up to 3 cm, Figure 4). Such reversible motion is observed in large parts of the study area, with more substantial magnitudes in the vicinity of the glacier tongue (see Figure S11 in the Supporting Information). The ascending and descending monthly timeseries of deformation correlate with the variation of the hydraulic head (Pearson's correlation coefficient of respectively 0.47 and 0.22) measured in the borehole B4 (see Figure 1). The deformation at the valley scale exhibits Pearson's correlation coefficients of respectively 0.57 and 0.62 with two months lag to the monitored hydraulic head (see Figure 5) and even coefficients of 0.62 and 0.75 when discarding winter times. While the depth at which the hydraulic head is monitored in the borehole is relatively shallow ($\sim$45 m), it reacts rapidly to recharge from the surface (Hugentobler et al., 2020).

By knowing the average direction of the groundwater-related displacement in the region from Oestreicher et al. (2021), we can combine the information from the ascending and descending orbits and estimate the displacement magnitude and orientation with Figure S10 in the Supporting Information. In Figure 6, we jointly analyze the information derived from cGNSS, RTS, and DInSAR ascending and descending orbits along the two profiles shown in Figure 4. The interpretation from the satellite displacement directions (black arrows) correlates well with the ones drawn from cGNSS and RTS observations performed on the left flank of the glacier. It complements these data for regions not covered by the other methods. Noteworthy, we found that the interpreted seasonal DInSAR displacement dynamics are generally underestimated compared to the grounded-based observations (see Figure 6). This bias might be due to different processes occurring locally, challenging the signal decomposition algorithm and leading to a cross-talk between the first and second ICs.

Our analysis with the vbICA method isolates a third independent component of displacement in the study area (see Figure S9 in the Supporting

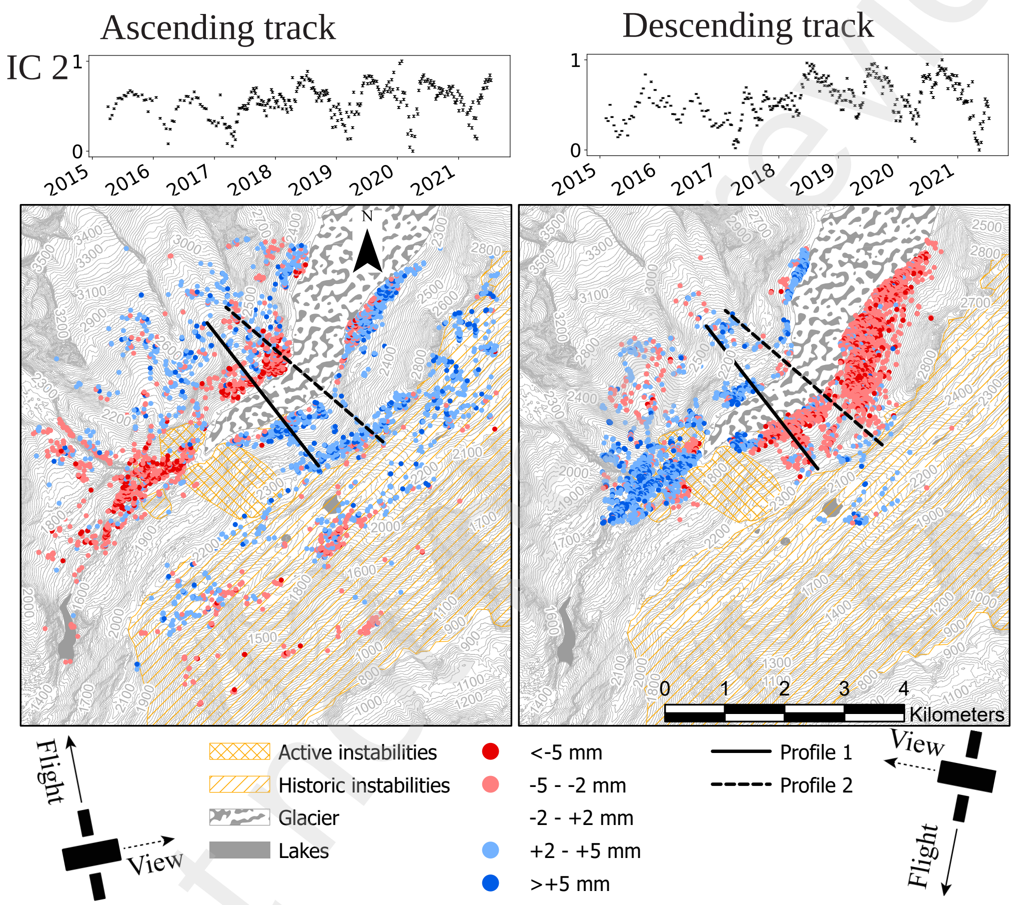

Figure 4: Second independent component of vbICA exhibits cyclic annual displacement for the ascending and descending tracks of the satellite. The upper panels show the time series related to the IC. Positive values on the map signify displacement towards the satellite for a positive change in the time series.

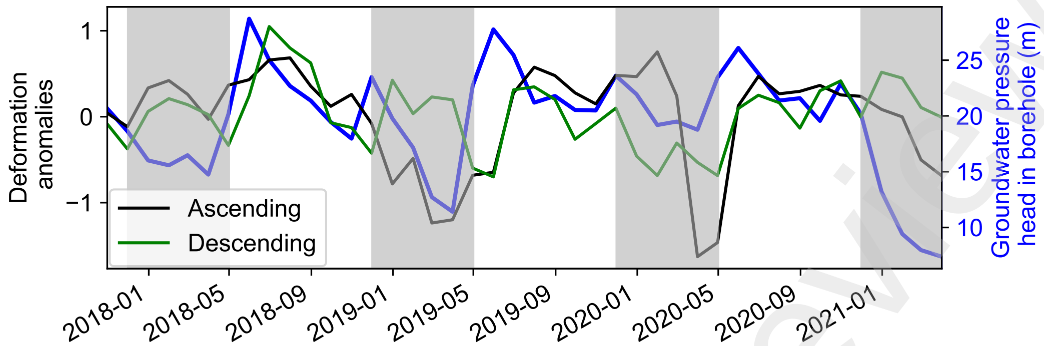

Figure 5: Comparison between the monthly deformation anomalies (ascending orbit, black and descending orbit, green) and the monthly pressure head at B4 (blue). Grey areas are periods with expected partial snow coverage, during which lower correlation factors may be expected because of decorrelation induced by the snow.

Information). It shows a low magnitude of displacement, with only some points over 2 mm for the ascending orbit. The temporal pattern exhibits an annual cyclicity.

4. Discussion and Conclusion

The results of the interferometric point target analysis (IPTA) show that the method can monitor sub-centimetric surface displacement in complex alpine environments, such as the Aletsch valley. One of the main challenges of the IPTA method is that parts of the hillslopes cannot be monitored due to geometrical decorrelation (e.g., Rosen et al., 2000). In addition, slope displacements that are too fast (>1.4 cm in LOS between two scenes for Sentinel 1) or oriented approximately perpendicularly to the satellite LOS also cannot be monitored efficiently (Manconi, 2021). At our study site, we could show that the IPTA method could detect Persistent Scatterers (PS) away from the reference point across decorrelated parts on the opposite side of large slope instabilities and the glacier. Positioning the reference at a location where the displacement is known, i.e., a cGNSS station in our case, helps correct the IPTA dataset with the displacement of the reference point. The comparison with the other surface displacement monitoring systems at our study site (GNSS and total stations) shows good correlations that validate the accuracy of the satellite-based measurements (Figure 2).

The challenge when analyzing the surface displacement timeseries is the decomposition of the signal in different spatiotemporal patterns that can be

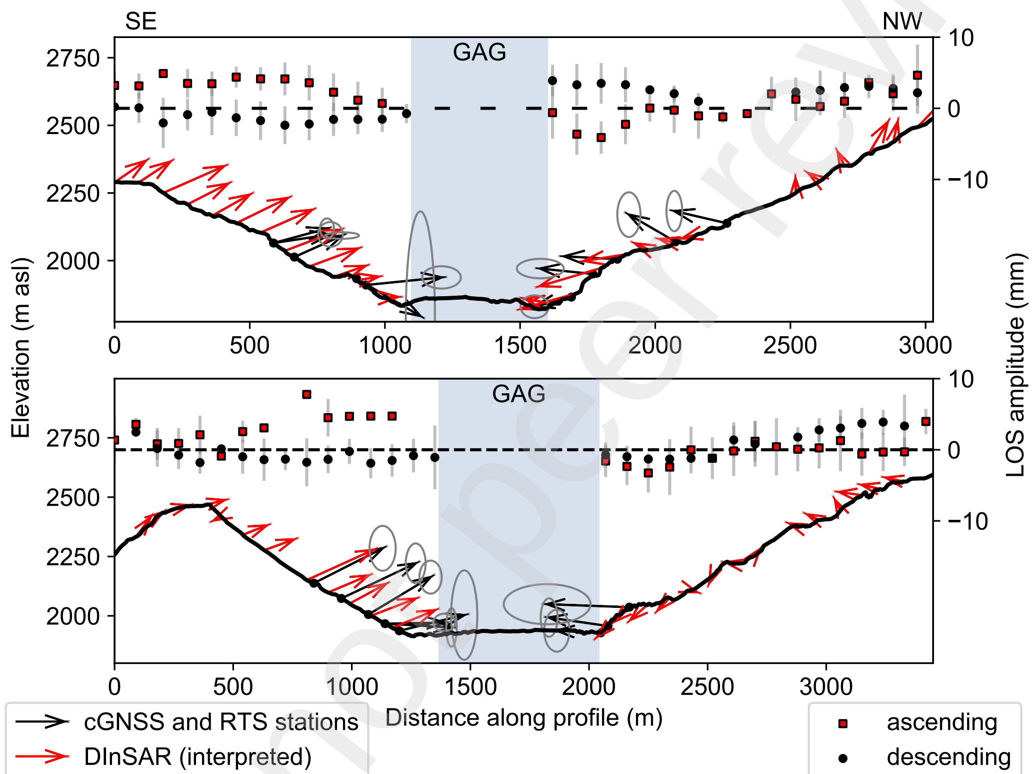

Figure 6: Topographic profiles across the valley with groundwater-related displacement during infiltration. Top: profile 1; Bottom: profile 2 in Figure 4. Black arrows are cGNSS and RTS data (grey ellipses for uncertainty). Red arrows are interpreted direction of ground displacement from DInSAR, and points are raw data from Figure 4 with a 90 m buffer distance around the profile. GAG stands for Great Aletsch Glacier, and its extent is delimited in blue.

related to environmental processes. Different statistical approaches exist to reduce the dimensionality of the dataset, including vbICA (Gualandi and Liu, 2021; Larochelle et al., 2022). While these approaches have been mainly applied at large-scale (Serpelloni et al., 2018), we show a successful signal decomposition with the vbICA method at hillslope scale in a complex alpine environment. This approach decomposes the signal into three independent components (IC) based on the Automatic Relevance Determination method (Gualandi and Liu, 2021). The first IC is mainly composed of a linear trend, with a superimposed weak annual cyclic pattern (see Figure 7). The linear trend is interpreted to be a long-term mechanical response of the slopes, while the weak seasonal signal is likely to be a residual of the seasonal cycles identified in IC2, which is discussed later. At certain locations, the long-term trends are oriented downslope and represent the long-term gravitational slope motion. We do not only observe such slow surface displacements on mature landslides but also on slopes at early stages of damage accumulation. For example, we identify long-term gravitational slope motion close to the Moosfluh and Driest instabilities (Glueer et al., 2019, 2020; Kos et al., 2016). Numerical experiments have shown that the Moosfluh and Driest instabilities are likely caused by cycles of glacier advance and retreat that induce progressive damage in the surrounding slopes (Grämiger et al., 2017). In addition, temperature (Grämiger et al., 2018; Hugentobler et al., 2021) and groundwater fluctuations (Grämiger et al., 2020; Hugentobler et al., 2022) have been identified as important factors contributing to the long-term damage of the slopes. The modeled damage is significantly greater when the temperature effect is taken into account (Grämiger et al., 2018), as rocks are rapidly exposed to warmer conditions (paraglacial thermal shock, (Grämiger et al., 2018)) and more short-term temperature fluctuations after the ice retreats (Hugentobler et al., 2021). With annual groundwater table fluctuations included, damage also increases due to hydromechanical fatigue, and the mode of failure in the model resembles the landslide observations in the Aletsch valley (Grämiger et al., 2020). The strongest damage occurs directly at the glacier margin and moves down (or up) the slope with the pace of glacier retreat (or advance) during multiple glacial cycles (Hugentobler et al., 2022). We also observe significant long-term trends in the signal of PS located on a relict rock glacier to the east of the GNSS station AL03. In this case, it can be attributed to the long-term creep of the rock glacier (Marcer et al., 2021; Harris et al., 2009).

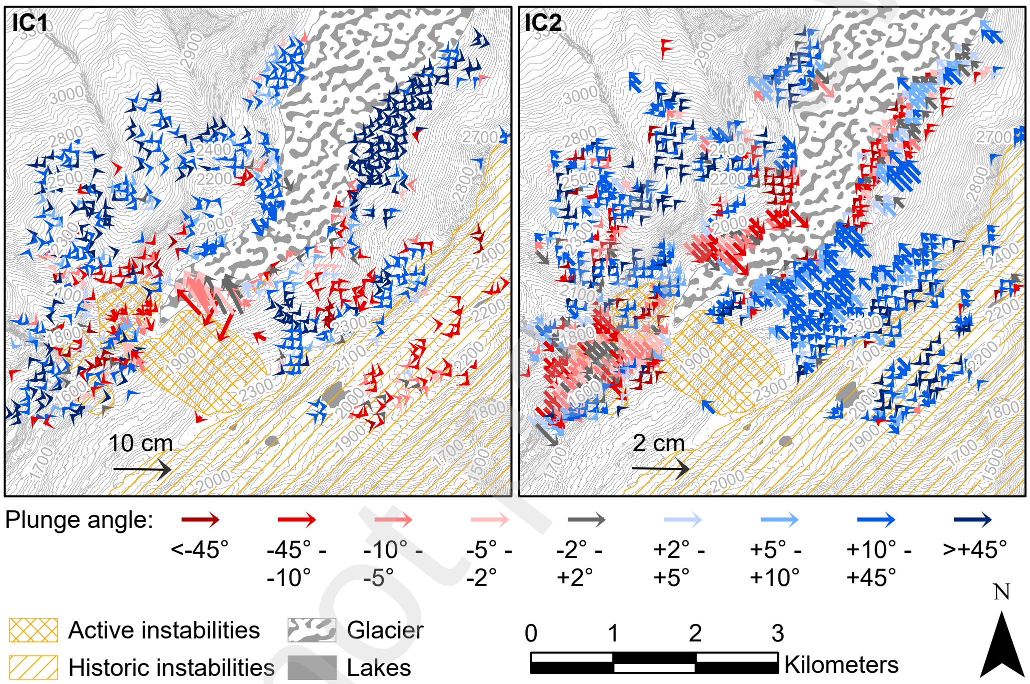

Figure 7: Displacement obtained by combining the ascending and descending orbits with the local average slope direction for the first IC (left) and with the average dip direction of the foliation for the second IC (right) of the vbICA method. The arrows show the horizontal orientation of displacement and magnitude (long-term trend for IC1, during recharge for IC2), and the colors display the plunge angle of the displacement.

In slopes not influenced by significant gravitational movements, the signal decomposition reveals an uplift close to the current glacier margins (Figure 3). This uplift is interpreted to be caused by the elastic isostatic rebound of the bedrock as a response to the contemporary glacier retreat (Hugentobler et al., 2022; Erfani Jazi et al., 2022). In the Ze Bächu region, the PS uplift is on average 2 mm/yr and up to 5 mm/yr. This uplift rate is confirmed by ground-truth measurements of nearby reflectors measured by the total station. In the Northeastern part of the study area, the left flank of the glacier exhibits high plunge angles and uplift rates around 0.8 mm/yr to 1 mm/yr. The large horizontal motion recorded at Ze Bächu (average of 5.7 mm/yr for PS close to the glacier) and around the cGNSS stations AL03 and ALTS on the other valley flank is interpreted as caused by hydromechanical fatigue in part (Oestreicher et al., 2021). Newly identified locations with large gravitational displacements superposed on the glacial elastic rebound, North-East of the Driest instability, North-East of Chatzulecher, and on the right flank of the Moosfluh instability highlight zones with a potential to transition towards unstable slopes.

The second IC shows a reversible cyclic displacement. Such deformation dynamics have been previously identified with ground-based stations and attributed to pore pressure variations during groundwater recharge-discharge cycles (Dal Moro and Zadro, 1998; Lesparre et al., 2017; Serpelloni et al., 2018; Grillo et al., 2018; Braitenberg et al., 2019; Oestreicher et al., 2021). They are caused by changes in pore pressure in the rock mass linked to the strong seasonal dynamics of hydrologic cycles in alpine environments (Gleeson and Manning, 2008; Markovich et al., 2019; Somers and McKenzie, 2020). Indeed, at high elevations, groundwater recharge is mainly controlled by snowmelt in spring (Barnett et al., 2005; Manning et al., 2012), with high magnitude of water table rise (de Palézieux and Loew, 2019). After recharge stops, groundwater is progressively discharged towards the receiving stream and springs network, associated with a decrease in the pore pressure (de Palézieux and Loew, 2019; Hugentobler et al., 2020). The natural pore pressure variations induce deformation of the valley slopes (Oestreicher et al., 2021; Chaussard and Farr, 2019). We constrain the displacement in a vertical plane perpendicular to the average direction of the main alpine foliation (approximately 136 deg) in Figure 7. Indeed, Oestreicher et al. (2021) showed that the displacement of cGNSS stations and total station reflectors in the valley was strongly influenced by the orientation of the alpine foliation. While the displacement in Spring is generally oriented upwards or horizontally out of the slope (see Figure 7), downwards-oriented displacements or displacements toward the mountains are also found. Such signals are often situated at locations that also experience substantial linear displacements in IC1. The minor seasonal deformation contained in IC1 impacts the results of IC2, such that it erroneously identifies a signal in the opposite direction as compensation for the more significant amplitude signal of IC1. Such an intricate signal could also explain the discrepancies between the displacement recorded by the total station's reflectors and IC2 around the station AL02 (see Figure 6).

In Figure 5, we compare the borehole water pressure head with satellite-based displacements of the slopes, and we find a good correlation with a slight time-lag between the peak in the groundwater table and the peak in deformation observed from the satellite. The time lag reveals a shorter response timescale measured in the shallow subsurface by the borehole location with respect to the one observed from the satellite-based deformation. The hydraulic diffusivity of the shallower part of the bedrock is generally higher than that of the overall rock mass at depth (Welch and Allen, 2014; Roques et al., 2022). This is due to a denser fracture network with high permeability close to the surface, with channelized groundwater flow. The delay observed in the deformation pattern is interpreted to be caused by the overall rock mass having a lower diffusivity and bulk permeability. This has been investigated in previous studies hypothesizing that the deformation is caused by changes in pore pressure up to a depth of at least a few hundred meters, greater than the borehole B4 depth (Oestreicher et al., 2021, 2023). A numerical experiment with an elastic hydromechanical model showed that the fracture network characteristics strongly control the deformation pattern observed at the surface (Oestreicher et al., 2023). The pore pressure-induced displacement is oriented horizontally or slightly downwards, close to the valley center and the glacier. In contrast, it is generally oriented upwards for PS situated higher on the slopes (see Figure 7), following the projections of conceptual numerical models (Oestreicher et al., 2023).

We interpret the third independent component with its low-magnitude displacement signal as a potential residual of the previously discussed groundwater-related motion or atmospheric noise in the satellite data. If attributed to pore pressure-induced deformation, this would indicate a non-stationary spatial pattern for the groundwater distribution. This can be the case, given the cross-talk between the first two ICs. Given the small amplitude of IC3, we cannot claim a physical origin for it with certainty. In fact, another difficulty and source of noise in the area is the changing elevation around the glacier due to the ice removal. We processed the dataset with a single digital elevation model (DEM), inducing possible errors for points next to the glacier and recently uncovered.

The spatial variations of pore pressure-related surface deformation in the study area provide precious information about the groundwater flow in mountain slopes (e.g., Neely et al., 2021), which is challenging to acquire directly in such remote environments (Hugentobler et al., 2020). In general, we report good agreement with the direction and magnitude at cGNSS and total stations (see Figure 6 and (Oestreicher et al., 2021)), except for locations with a large amplitude of long-term trends. The more extensive spatial coverage of DInSAR allows for broadening the analysis to a larger slope area than traditional measurements like cGNSS or total stations. It indicates that the hydraulic response zone in the study area integrates a large volume of the mountain slope at a maximal depth of approximately 500 m in our case.

We demonstrate that we can isolate signals in satellite data in remote alpine areas around a glacier and large slope instabilities. We show that the hydromechanically active structures respond at seasonal scales to recharge and discharge in fractured bedrock aquifers. Our results show that remote sensing satellite data can be used to study mechanisms of slope surface displacements in remote alpine areas. This study opens the possibility of utilizing satellites, together with ground-truthing stations and coherent structural hypotheses, to investigate other remote areas that are less heavily instrumented.

Declaration of Interests

The authors declare that they have no known competing financial interests or personal relationships that could have appeared to influence the work reported in this paper.

Acknowledgments

This project is funded by the Swiss National Science Foundation (project 172492). We thank GAMMA Remote Sensing AG for significant help in the IPTA processing. We thank the many field assistants who gave their time for this project through the years. We thank colleagues and friends for their support.

Appendix A. Supporting Information

Supporting Information for this article can be found online at (DOI and will be added here for the supporting information file once the manuscript has been accepted for publication).

References

Agliardi, F., Scuderi, M.M., Fusi, N., Collettini, C., 2020. Slow-to-fast transition of giant creeping rockslides modulated by undrained loading in basal shear zones. Nature Communications 11, 1–11. URL: http://dx.doi.org/10.1038/s41467-020-15093-3, doi:10.1038/s41467-020-15093-3.

Ali, M.Z., Chu, H., Tatas, Burbey, T.J., 2022. Estimation of annual groundwater changes from InSAR-derived land subsidence. Water and Environment Journal , 1–11URL: https://onlinelibrary.wiley.com/doi/10.1111/wej.12802, doi:10.1111/wej.12802.

Ballantyne, C.K., Wilson, P., Gheorghiu, D., Rodés, A., 2014. Enhanced rock-slope failure following ice-sheet deglaciation: timing and causes. Earth Surface Processes and Landforms 39, 900–913. URL: https://onlinelibrary.wiley.com/doi/full/10.1002/esp.3495 https://onlinelibrary.wiley.com/doi/abs/10.1002/esp.3495 https://onlinelibrary.wiley.com/doi/10.1002/esp.3495, doi:10.1002/esp.3495.

Barnett, T.P., Adam, J.C., Lettenmaier, D.P., 2005. Potential impacts of a warming climate on water availability in snow-dominated regions. Nature 438, 303–309. URL: https://doi.org/10.1038/nature04141 http://www.nature.com/articles/nature04141, doi:10.1038/nature04141.

Béjar-Pizarro, M., Ezquerro, P., Herrera, G., Tomás, R., Guardiola-Albert, C., Ruiz Hernández, J.M., Fernández Merodo, J.A., Marchamalo, M., Martínez, R., 2017. Mapping groundwater level and aquifer storage variations from InSAR measurements in the Madrid aquifer, Central Spain. Journal of Hydrology 547, 678–689. URL:

https://linkinghub.elsevier.com/retrieve/pii/S0022169417300896, doi:10.1016/j.jhydrol.2017.02.011.

Berger, A., Mercolli, I., Herwegh, M., Gnos, E., 2016. Geological Map of the Aar Massif, Tavetsch and Gotthard Nappes. - Geol. spec. Map 1:100000, map sheet 129.

Bock, Y., Agnew, D.C., Fang, P., Genrich, J.F., Hager, B.H., Herring, T.A., Hudnut, K.W., King, R.W., Larsen, S., Minster, J.B., Stark, K., Wdowinski, S., Wyatt, F.K., 1993. Detection of crustal deformation from the Landers earthquake sequence using continuous geodetic measurements. Nature 361, 337–340. doi:10.1038/361337a0.

Braitenberg, C., Pivetta, T., Barbolla, D.F., Gabrovšek, F., Devoti, R., Nagy, I., 2019. Terrain uplift due to natural hydrologic overpressure in karstic conduits. Scientific Reports 9, 3934. URL: http://www.nature.com/articles/s41598-019-38814-1, doi:10.1038/s41598-019-38814-1.

Chaussard, E., Farr, T.G., 2019. A New Method for Isolating Elastic From Inelastic Deformation in Aquifer Systems: Application to the San Joaquin Valley, CA. Geophysical Research Letters 46, 10800–10809. URL: https://onlinelibrary.wiley.com/doi/abs/10.1029/2019GL084418, doi:10.1029/2019GL084418.

Choudrey, R.A., Roberts, S.J., 2003. Variational Mixture of Bayesian Independent Component Analyzers. Neural Computation 15, 213–252. doi:10.1162/089976603321043766.

Collins, B.D., Stock, G.M., Eppes, M.C., Lewis, S.W., Corbett, S.C., Smith, J.B., 2018. Thermal influences on spontaneous rock dome exfoliation. Nature Communications 9, 1–12. URL: http://dx.doi.org/10.1038/s41467-017-02728-1, doi:10.1038/s41467-017-02728-1.

Crosetto, M., Monserrat, O., Cuevas-González, M., Devanthéry, N., Crippa, B., 2016. Persistent Scatterer Interferometry: A review. ISPRS Journal of Photogrammetry and Remote Sensing 115, 78–89. doi:10.1016/J.ISPRSJPRS.2015.10.011.

Dal Moro, G., Zadro, M., 1998. Subsurface deformations induced by rainfall and atmospheric pressure: Tilt/strain measurements in the NE-Italy seismic area. Earth and Planetary Science Letters doi:10.1016/S0012-821X(98)00203-9.

Ebmeier, S.K., 2016. Application of independent component analysis to multitemporal InSAR data with volcanic case studies. Journal of Geophysical Research: Solid Earth 121, 8970–8986. doi:10.1002/2016JB013765.

Erfani Jazi, Z., Motagh, M., Klemann, V., 2022. Inferring Mass Loss by Measuring Contemporaneous Deformation around the Helheim Glacier, Southeastern Greenland, Using Sentinel-1 InSAR. Remote Sensing 14, 3956. URL: https://www.mdpi.com/2072-4292/14/16/3956, doi:10.3390/rs14163956.

Frukacz, M., Presl, R., Wieser, A., Favot, D., 2017. Pushing the sensitivity limits of RTS-based continuous deformation monitoring of an alpine valley. Applied Geomatics 9, 81–92. URL: https://doi.org/10.1007/s12518-017-0182-2, doi:10.1007/s12518-017-0182-2.

Gaddes, M.E., Hooper, A., Bagnardi, M., Inman, H., Albino, F., 2018. Blind Signal Separation Methods for InSAR: The Potential to Automatically Detect and Monitor Signals of Volcanic Deformation. Journal of Geophysical Research: Solid Earth 123, 226–10. doi:10.1029/2018JB016210.

GLAMOS - Glacier Monitoring Switzerland, 2021. Swiss Glacier Length Change (release 2021).

Gleeson, T., Manning, A.H., 2008. Regional groundwater flow in mountainous terrain: Three-dimensional simulations of topographic and hydrogeologic controls. Water Resources Research 44. URL: https://agupubs.onlinelibrary.wiley.com/doi/abs/10.1029/2008WR006848 http://doi.wiley.com/10.1029/2008WR006848, doi:10.1029/2008WR006848.

Glueer, F., Loew, S., Manconi, A., 2020. Paraglacial history and structure of the Moosfluh Landslide (1850–2016), Switzerland. Geomorphology 355, 106677. URL: https://www.sciencedirect.com/science/article/pii/S0169555X19300558 https://linkinghub.elsevier.com/retrieve/pii/S0169555X19300558, doi:10.1016/j.geomorph.2019.02.021.

Glueer, F., Loew, S., Manconi, A., Aaron, J., 2019. From Toppling to Sliding: Progressive Evolution of the Moosfluh Landslide, Switzerland. Journal of Geophysical Research: Earth Surface 124, 2899–2919. URL: https://onlinelibrary.wiley.com/doi/abs/10.1029/2019JF005019, doi:10.1029/2019JF005019.

Glueer, F., Loew, S., Seifert, R., Aaron, J., Grämiger, L., Conzett, S., Limpach, P., Wieser, A., Manconi, A., 2021. Robotic Total Station Monitoring in High Alpine Paraglacial Environments: Challenges and Solutions from the Great Aletsch Region (Valais, Switzerland). Geosciences 11, 471. URL: https://www.mdpi.com/2076-3263/11/11/471, doi:10.3390/geosciences11110471.

Grämiger, L.M., Moore, J.R., Gischig, V.S., Ivy-Ochs, S., Loew, S., 2017. Beyond debuttressing: Mechanics of paraglacial rock slope damage during repeat glacial cycles. Journal of Geophysical Research: Earth Surface 122, 1004–1036. URL: http://doi.wiley.com/10.1002/2016JF003967, doi:10.1002/2016JF003967.

Grämiger, L.M., Moore, J.R., Gischig, V.S., Loew, S., 2018. Thermomechanical Stresses Drive Damage of Alpine Valley Rock Walls During Repeat Glacial Cycles. Journal of Geophysical Research: Earth Surface 123, 2620–2646. URL: http://doi.wiley.com/10.1029/2018JF004626, doi:10.1029/2018JF004626.

Grämiger, L.M., Moore, J.R., Gischig, V.S., Loew, S., Funk, M., Limpach, P., 2020. Hydromechanical Rock Slope Damage During Late Pleistocene and Holocene Glacial Cycles in an Alpine Valley. Journal of Geophysical Research: Earth Surface 125, 1–24. URL: https://onlinelibrary.wiley.com/doi/10.1029/2019JF005494, doi:10.1029/2019JF005494.

Grillo, B., Braitenberg, C., Nagy, I., Devoti, R., Zuliani, D., Fabris, P., 2018. Cansiglio Karst Plateau: 10 Years of Geodetic-Hydrological Observations in Seismically Active Northeast Italy. Pure and Applied Geophysics 175, 1765–1781.

URL: http://link.springer.com/10.1007/s00024-018-1860-7, doi:10.1007/s00024-018-1860-7.

Gualandi, A., Liu, Z., 2021. Variational Bayesian Independent Component Analysis for InSAR Displacement Time-Series With Application to Central California, USA. Journal of Geophysical Research: Solid Earth 126. URL: https://agupubs.onlinelibrary.wiley.com/doi/full/10.1029/2020JB020845 https://agupubs.onlinelibrary.wiley.com/doi/abs/10.1029/2020JB020845 https://agupubs.onlinelibrary.wiley.com/doi/10.1029/2020JB020845 https://onlinelibrary.wiley.com/doi/10.1029/2020JB0, doi:10.1029/2020JB020845.

Harris, C., Arenson, L.U., Christiansen, H.H., Etzelmüller, B., Frauenfelder, R., Gruber, S., Haeberli, W., Hauck, C., Hölzle, M., Humlum, O., Isaksen, K., Kääb, A., Kern-Lütschg, M.A., Lehning, M., Matsuoka, N., Murton, J.B., Nötzli, J., Phillips, M., Ross, N., Seppälä, M., Springman, S.M., Vonder Mühll, D., 2009. Permafrost and climate in Europe: Monitoring and modelling thermal, geomorphological and geotechnical responses. Earth-Science Reviews 92, 117–171. doi:10.1016/J.EARSCIREV.2008.12.002.

Hugentobler, M., Aaron, J., Loew, S., 2021. Rock Slope Temperature Evolution and Micrometer-Scale Deformation at a Retreating Glacier Margin. Journal of Geophysical Research: Earth Surface 126, 1–33. URL: https://onlinelibrary.wiley.com/doi/10.1029/2021JF006195, doi:10.1029/2021JF006195.

Hugentobler, M., Aaron, J., Loew, S., Roques, C., 2022. Hydro-Mechanical Interactions of a Rock Slope With a Retreating Temperate Valley Glacier. Journal of Geophysical Research: Earth Surface 127. URL: https://onlinelibrary.wiley.com/doi/10.1029/2021JF006484, doi:10.1029/2021JF006484.

Hugentobler, M., Loew, S., Aaron, J., Roques, C., Oestreicher, N., 2020. Borehole monitoring of thermo-hydro-mechanical rock slope processes adjacent to an actively retreating glacier. Geomorphology 362, 107190. URL: https://doi.org/10.1016/j.geomorph.2020.107190, doi:10.1016/j.geomorph.2020.107190.

Huss, M., Hock, R., 2018. Global-scale hydrological response to future glacier mass loss. Nature Climate Change 8, 135–

140. URL: http://dx.doi.org/10.1038/s41558-017-0049-x http://www.nature.com/articles/s41558-017-0049-x, doi:10.1038/s41558-017-0049-x.

Kos, A., Amann, F., Strozzi, T., Delaloye, R., von Ruette, J., Springman, S., 2016. Contemporary glacier retreat triggers a rapid landslide response, Great Aletsch Glacier, Switzerland. Geophysical Research Letters doi:10.1002/2016GL071708.

Larochelle, S., Chanard, K., Fleitout, L., Fortin, J., Gualandi, A., Longuevergne, L., Rebischung, P., Violette, S., Avouac, J.p., 2022. Understanding the Geodetic Signature of Large Aquifer Systems: Example of the Ozark Plateaus in Central United States. Journal of Geophysical Research: Solid Earth 127, 1–29. URL: https://onlinelibrary.wiley.com/doi/10.1029/2021JB023097, doi:10.1029/2021JB023097.

Lesparre, N., Boudin, F., Champollion, C., Chéry, J., Danquigny, C., Seat, H.C., Cattoen, M., Lizion, F., Longuevergne, L., 2017. New insights on fractures deformation from tiltmeter data measured inside the Fontaine de Vaucluse karst system. Geophysical Journal International doi:10.1093/gji/ggw446.

Limpach, P., Geiger, A., Raetzo, H., 2016. GNSS for Deformation and Geohazard Monitoring in the Swiss Alps, in: Proceedings of the 3rd Joint International Symposium on Deformation Monitoring (JISDM 2016), Vienna, Vienna. pp. 1–4.

Loew, S., Ebneter, F., Bremen, R., Herfort, M., Lützenkirchen, V., Matousek, F., 2007. Annual Opening and Closure of Alpine Valleys. Felsbau : rock and soil engineering 25, 1–60. URL: https://structurae.net/en/literature/journal-article/annual-opening-and-closure-

Manconi, A., 2021. How phase aliasing limits systematic space-borne DInSAR monitoring and failure forecast of alpine landslides. Engineering Geology 287. doi:10.1016/J.ENGGEO.2021.106094.

Manconi, A., Kourkouli, P., Caduff, R., Strozzi, T., Loew, S., 2018. Monitoring surface deformation over a failing rock slope with the ESA sentinels: Insights from Moosfluh instability, Swiss Alps. Remote Sensing 10. doi:10.3390/rs10050672.

Manning, A.H., Clark, J.F., Diaz, S.H., Rademacher, L.K., Earman, S., Niel Plummer, L., 2012. Evolution of groundwater age in a mountain watershed over a period of thirteen years. Journal of Hydrology doi:10.1016/j.jhydrol.2012.06.030.

Marcer, M., Cicoira, A., Cusicanqui, D., Bodin, X., Echelard, T., Obregon, R., Schoeneich, P., 2021. Rock glaciers throughout the French Alps accelerated and destabilised since 1990 as air temperatures increased. Communications Earth & Environment 2. URL: https://www.nature.com/articles/s43247-021-00150-6, doi:10.1038/s43247-021-00150-6.

Markovich, K.H., Manning, A.H., Condon, L.E., McIntosh, J.C., 2019. Mountain-block Recharge: A Review of Current Understanding. Water Resources Research , 2019WR025676URL: https://onlinelibrary.wiley.com/doi/abs/10.1029/2019WR025676, doi:10.1029/2019WR025676.

Mey, J., Scherler, D., Wickert, A.D., Egholm, D.L., Tesauro, M., Schildgen, T.F., Strecker, M.R., 2016. Glacial isostatic uplift of the European Alps. Nature Communications 7, 13382. URL: http://www.nature.com/articles/ncomms13382, doi:10.1038/ncomms13382.

Neely, W.R., Borsa, A.A., Burney, J.A., Levy, M.C., Silverii, F., Sneed, M., 2021. Characterization of Groundwater Recharge and Flow in California's San Joaquin Valley From InSAR-Observed Surface Deformation. Water Resources Research 57. URL: https://onlinelibrary.wiley.com/doi/10.1029/2020WR028451, doi:10.1029/2020WR028451.

Oestreicher, N., Lei, Q., Loew, S., Roques, C., 2023. Bedrock Fractures Control Groundwater-Driven Mountain Slope Deformations. Journal of Geophysical Research: Earth Surface 128. doi:10.1029/2022JF006885.

Oestreicher, N., Loew, S., Roques, C., Aaron, J., Gualandi, A., Longuevergne, L., Limpach, P., Hugentobler, M., 2021. Controls on Spatial and Temporal Patterns of Slope Deformation in an Alpine Valley. Journal of Geophysical Research: Earth Surface 126. doi:10.1029/2021jf006353.

Oliva, M., Mercier, D., Ruiz-Fernández, J., McColl, S., 2020. Paraglacial processes in recently deglaciated environments. Land Degradation and Development 31, 1871–1876. doi:10.1002/ldr.3283.

de Palézieux, L., Loew, S., 2019. Long-term transient groundwater pressure and deep infiltration in Alpine mountain slopes (Poschiavo Valley, Switzerland). Hydrogeology Journal 27, 2817–2834. URL: http://link.springer.com/10.1007/s10040-019-02025-9, doi:10.1007/s10040-019-02025-9.

Roques, C., Rupp, D.E., De Dreuzy, J.R., Longuevergne, L., Jachens, E.R., Grant, G., Aquilina, L., Selker, J.S., 2022. Recession discharge from compartmentalized bedrock hillslopes. Hydrology and Earth System Sciences 26, 4391–4405. doi:10.5194/hess-26-4391-2022.

Rosen, P., Hensley, S., Joughin, I., Li, F., Madsen, S., Rodriguez, E., Goldstein, R., 2000. Synthetic aperture radar interferometry. Proceedings of the IEEE 88, 333–382. URL: http://ieeexplore.ieee.org/document/838084/, doi:10.1109/5.838084.

Rouet-Leduc, B., Jolivet, R., Dalaison, M., Johnson, P.A., Hulbert, C., 2021. Autonomous extraction of millimeter-scale deformation in InSAR time series using deep learning. Nature Communications 12, 6480. URL: http://arxiv.org/abs/2012.13849 https://www.nature.com/articles/s41467-021-26254-3, doi:10.1038/s41467-021-26254-3.

Serpelloni, E., Pintori, F., Gualandi, A., Scoccimarro, E., Cavaliere, A., Anderlini, L., Belardinelli, M.E., Todesco, M., 2018. Hydrologically Induced Karst Deformation: Insights From GPS Measurements in the Adria-Eurasia Plate Boundary Zone. Journal of Geophysical Research: Solid Earth doi:10.1002/2017JB015252.

Somers, L.D., McKenzie, J.M., 2020. A review of groundwater in high mountain environments. Wiley Interdisciplinary Reviews: Water 7, 1–27. doi:10.1002/wat2.1475.

Song, S., Bai, L., Yang, C., 2022. Characterization of the Land Deformation Induced by Groundwater Withdrawal and Aquifer Parameters

Using InSAR Observations in the Xingtai Plain, China. Remote Sensing 14, 4488. URL: https://doi.org/10.3390/rs14184488 https://www.mdpi.com/2072-4292/14/18/4488, doi:10.3390/rs14184488.

Sternai, P., Sue, C., Husson, L., Serpelloni, E., Becker, T.W., Willett, S.D., Faccenna, C., Di Giulio, A., Spada, G., Jolivet, L., Valla, P., Petit, C., Nocquet, J.M., Walpersdorf, A., Castelltort, S., 2019. Present-day uplift of the European Alps: Evaluating mechanisms and models of their relative contributions. Earth-Science Reviews 190, 589–604. doi:10.1016/j.earscirev.2019.01.005.

Storni, E., Hugentobler, M., Manconi, A., Loew, S., 2020. Geomorphology Monitoring and analysis of active rockslide-glacier interactions (Moosfluh , Switzerland). Geomorphology 371, 107414. URL: https://doi.org/10.1016/j.geomorph.2020.107414, doi:10.1016/j.geomorph.2020.107414.

Strozzi, T., Caduff, R., Wegmüller, U., Raetzo, H., Hauser, M., 2017. Widespread surface subsidence measured with satellite SAR interferometry in the Swiss alpine range associated with the construction of the Gotthard Base Tunnel. Remote Sensing of Environment 190, 1–12. URL: http://dx.doi.org/10.1016/j.rse.2016.12.007, doi:10.1016/j.rse.2016.12.007.

Torres, R., Snoeij, P., Geudtner, D., Bibby, D., Davidson, M., Attema, E., Potin, P., Rommen, B., Floury, N., Brown, M., Traver, I.N., Deghaye, P., Duesmann, B., Rosich, B., Miranda, N., Bruno, C., L'Abbate, M., Croci, R., Pietropaolo, A., Huchler, M., Rostan, F., 2012. GMES Sentinel-1 mission. Remote Sensing of Environment 120, 9–24. doi:10.1016/J.RSE.2011.05.028.

Truttmann, S., Herwegh, M., Schreurs, G., Ebert, A., Hardmeier, S., 2021. The effect of pre-existing structures on the Moosfluh landslide and its lateral propagation (Great Aletsch Glacier, Switzerland). Geomorphology 377, 107530. URL: https://doi.org/10.1016/j.geomorph.2020.107530 https://linkinghub.elsevier.com/retrieve/pii/S0169555X20305031, doi:10.1016/j.geomorph.2020.107530.

Vasco, D.W., Farr, T.G., Jeanne, P., Doughty, C., Nico, P., 2019. Satellite-based monitoring of groundwater depletion in California's Central Valley. Scientific Reports 9, 1–14. URL: http://dx.doi.org/10.1038/s41598-019-52371-7, doi:10.1038/s41598-019-52371-7.

Vogler, M., 2015. Hydro-mechanical interactions between the Great Aletsch Glacier and the Driest landslide (Switzerland).

Wasowski, J., Bovenga, F., 2014. Investigating landslides and unstable slopes with satellite Multi Temporal Interferometry: Current issues and future perspectives. Engineering Geology 174, 103–138. doi:10.1016/J.ENGGEO.2014.03.003.

Wegmüller, U., Magnard, C., Werner, C., Strozzi, T., Caduff, R., Manconi, A., 2021. Methods to avoid being affected by non-zero closure phase in InSAR time series analysis in a multi-reference stack. Procedia Computer Science 181, 511–518. doi:10.1016/J.PROCS.2021.01.197.

Wegmüller, U., Werner, C., Strozzi, T., Wiesmann, A., Frey, O., Santoro, M., 2016. Sentinel-1 Support in the GAMMA Software. Procedia Computer Science 100, 1305–1312. doi:10.1016/j.procs.2016.09.246.

Welch, L.A., Allen, D.M., 2014. Hydraulic conductivity characteristics in mountains and implications for conceptualizing bedrock groundwater flow. Hydrogeology Journal 22, 1003–1026. URL: http://link.springer.com/10.1007/s10040-014-1121-5, doi:10.1007/s10040-014-1121-5.

Werner, C., Wegmüller, U., Strozzi, T., Wiesmann, A., 2003. Interferometric Point Target Analysis for Deformation Mapping. International Geoscience and Remote Sensing Symposium (IGARSS) 7, 4362–4364. doi:10.1109/igarss.2003.1295516.